2.36 at a static pressure of 115 torr. In both tests, the energy input to the spark was 1.45 joules, and the time delay 50 μsec. For the tunnel in operation, similarities between the disturbances viewed in planview and in profile are clearly apparent.

The main drawback of the planview shadowgraph technique in its present form proved to be its inability to show anything but the strongest boundary-layer disturbances, due to the masking effect of the boundary layer on the inside surface of the wind-tunnel window. It would be highly desirable to perfect this technique to the point where the finer details of the boundary layer could be observed in planview. For example, boundary-layer transition could be observed similarly to the way in which Emmons observed the appearance of turbulent spots in shallow water.[2] To achieve this, it is suggested that a) the focal length of the spherical mirror and consequently its f-stop be increased substantially to reduce the depth of field and permit minimizing the disturbance from the window boundary layer, and b) that the turbulent boundary at the near wind-tunnel wall be bled away upstream of the window, leaving only a thin, newly formed, boundary layer covering the inside surface of the window. While neither of these refinements is simple or inexpensive, the potential rewards in terms of basic information on boundary-layer behavior may still warrant their implementation, particularly since no other techniques with such capabilities are known.

References

[1] Klein, E. J., "Excitation of Boundary-Layer Turbulence Through Spark Discharges," NASA Ames Research Center (report in preparation).

[2] Emmons, H. W., "The Laminar-Turbulent Transition in a Boundary Layer-Part I," *Journal of the Aeronautical Sciences*, Vol. 18, No. 7, July 1951, pp. 490–498.

Condensation in Carbon Dioxide Jet Plumes

ALFRED E. BEYLICH*
NASA Marshall Space Flight Center, Huntsville, Ala.

CONSIDERABLE difficulties exist in calculating the flowfield of jet plumes such as those that issue from the attitude control engines of space stations, especially if condensation and changes in the specific heats occur in the flow. In order to obtain information about the condensation in these plumes, a simple experimental approach was made.

A model nozzle (0.56 mm throat diam, 11° half angle, and 40:1 exit to throat area) was used to produce a CO_2 jet plume in a vacuum chamber with LN_2 cooled cryogenic panels. With a chamber background pressure of about 10^{-4} torr, a ratio of stagnation to background pressure, p_0/p_∞, could be maintained up to 10^8. Nozzle wall temperature T_w and stagnation temperature T_0 were controlled. The use of CO_2 has, apart from the ease of cryopumping very large mass flows, importance because 40–60% of actual combustion products in control engines consist of CO_2 plus H_2O. Thus condensation effects in the flow can be fairly well simulated and studied.

Received October 27, 1969; revision received February 4, 1970. Research was accomplished while the author held a NRC Postdoctoral Resident Research Associateship supported by MSFC. The author wants to thank J. L. Sims from MSFC for making available his calculations and the staff of the Aero-Astrodynamics Laboratory for making these experiments possible.

* Resident Research Associate; presently on leave from Technische Hochschule, Aachen, Germany.

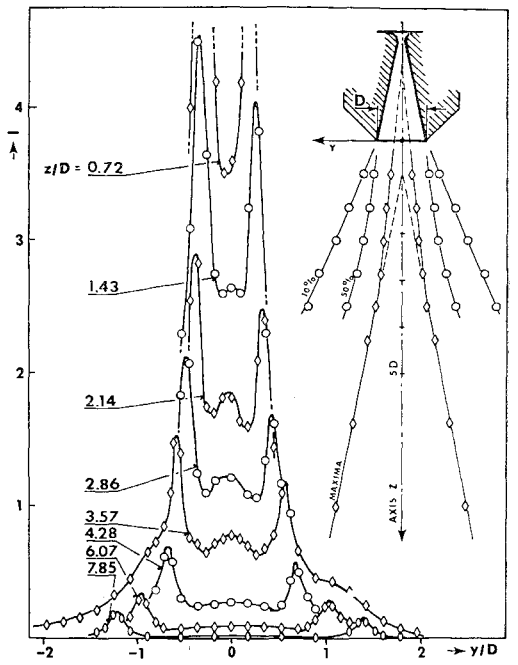

Fig. 1 Distribution of scattered light intensity (arbitrary units) at different distances z from the nozzle exit for stagnation pressure P_0 = 8 bar, stagnation temperature T_0 = 293°K, and chamber background pressure $P_\infty = 10^{-4}$ torr.

Light scattering, which is a simple and often applied method,[1,2] was used to detect the condensation. A He-Ne-laser and a photomultiplier were arranged with each of their optical axes perpendicular to the plume axis. The nozzle could be moved in three directions so that it was possible to measure the intensity of the scattered light at different points in the flow. By rotating the plane of polarization of the incident beam, one is able to make a first estimation about the particle size. In all experiments, this yielded a typical Rayleigh-type scattering. Thus the particle radius must be smaller than 6328 Å/2π. In the case of Rayleigh scattering one can only measure the product $n \cdot r^6$, where n is the number density and r a weighted mean radius of the condensed clusters. Thus knowledge of the amount of condensed mass is necessary to interpret the intensity measurements. In some cases this information can be obtained from calculation. Absolute values of $n \cdot r^6$ were obtained by comparing the intensity of the scattered light with the intensity of one pinhole of known size.

For an isentropic expansion[3] the vapor pressure line is crossed at about Mach 2, for p_0 = 1 — 10 bar and T_0 = 300°K, thus condensation should start slightly downstream the throat. The supersaturation required for starting the nucleation will move the condensation zone a small distance more downstream, but it will remain inside the nozzle. Thus condensation should, at low temperatures T_0, always be detected right up to the nozzle exit.

A survey of the intensity measurements in the jet plume is given in Fig. 1. A remarkable property of the scans arcoss the plume are the two peaks that appear on either side of the axis. The position of these maxima relative to the nozzle is shown on the right-hand side of Fig. 1, as well as the lines of 50 and 10% intensity, compared to the intensity $I(z,y = 0)$ on the axis. The influence of the stagnation temperature, T_0, on the intensity distribution across the plume at a fixed distance of 2.86 nozzle exit diam D is given in Fig. 2. With rising temperature T_0 the peaks move closer together; finally they merge to one peak and two additional side peaks appear. If one keeps the stagnation temperature constant

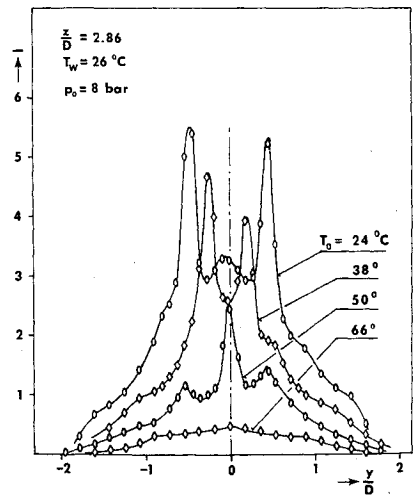

Fig. 2 Intensity distributions at a distance z = 2.86 nozzle exit diameters from the exit for different stagnation temperatures T_0.

and raises the pressure p_0 (Fig. 3), the two peaks become more marked, and the distance between them grows slightly.

Measurements in jet plumes produced by a sonic orifice showed no peaks but only a smooth bell-shaped profile. Since one-dimensional calculations[4] for the inside of the nozzle indicate a very slow growth of the clusters, these peaks are possibly a result of variations in the nucleation rate across the condensation zone, and not a result of different growth rates. This nucleation rate is strongly influenced by changes in the temperature. Another possibility may be a separation effect due to temperature gradients inside the nozzle.

Intensity measurements along the axis of the plume, as shown in Fig. 4 for different pressures p_0, allow an extrapolation into the nozzle exit plane. If one calculates, for instance for p_0 = 8 bar, the equilibrium value of the fraction of condensed mass at the exit, one obtains for the average particle radius and the number density the following values:

$$r_{(z=0)} = 20 \text{ Å}, \quad n_{(z=0)} = 5 \cdot 10^{14} \text{ clusters/cm}^3$$

One-dimensional calculations yield a value of r = 30–40 Å, using an accommodation coefficient of 1.0.

The particle growth outside the nozzle can be calculated from the measurements in the following manner: The intensity is given by

$$I = \text{const}_1 \cdot n \cdot r^6 \tag{1}$$

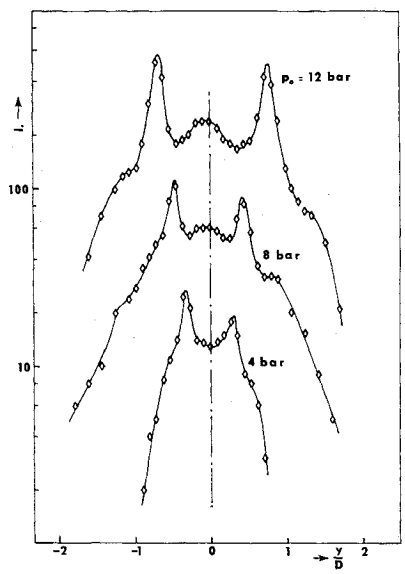

Fig. 3 Intensity distributions at a distance z = 2.86 D from nozzle exit for different stagnation pressures P_0.

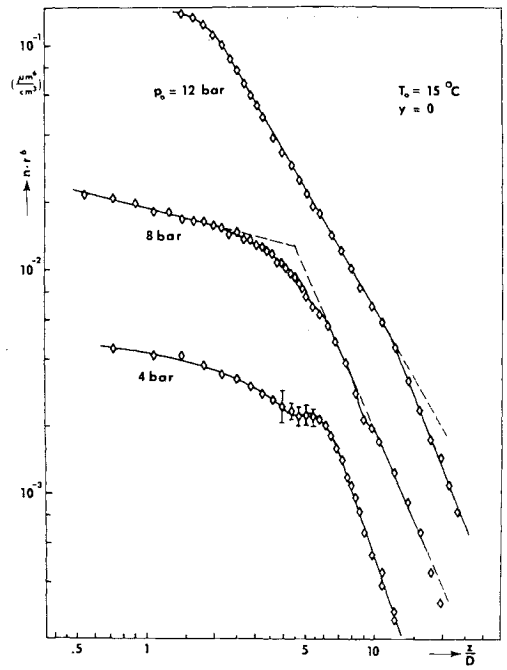

Fig. 4 Intensity, $n \cdot r^6$ (n = number density, r = particle radius) along the jet axis z for different stagnation pressures P_0. Stagnation temperature T_0 and nozzle wall temperature T_w are kept constant.

and the total change along the axis z is

$$dI/dz = (\partial I/\partial n)dn/dz + (\partial I/\partial r)dr/dz \tag{2}$$

Since the particles, after having left the nozzle, have essentially reached their final speed, one can obtain the dependence of the number density n on z by approximating a small part of the flow by the source flow relation

$$n = \text{const}_2 \cdot (z - z_0)^{-2} \tag{3}$$

where z_0 is the origin of the source flow. The location of $z_0(z)$ can be obtained graphically from Fig. 1 by assuming that the peaks in the flow follow stream lines. The change of particle radius r is then

$$d \ln r/d \ln z = \tfrac{1}{6}[d \ln I/d \ln z + 2z/(z - z)] \tag{4}$$

For the case of p_0 = 8 bar, the expression $d \ln I/d \ln z$ was obtained from Fig. 4, and $z_0(z)$ from Fig. 1. Graphical integration shows a very small growth speed at the exit that decreases continuously and goes toward zero at a distance of about 4D downstream from the exit. The over-all growth from the nozzle exit downstream is not more than 20%.

To summarize these preliminary results: the condensed particles are of small size and they grow, outside the nozzle, very slowly. The measurements at the nozzle exit compared well with one-dimensional calculations, but, from the appearance of the two off-axis peaks in the scattered light intensity measurements, one should be cautious about extending the one-dimensional results to a two-dimensional flowfield.

References

[1] Durbin, E. J., "Optical Methods Involving Light Scattering for Measuring Size and Concentration of Condensation Particles in Supercooled Hypersonic Flow," TN 2441, 1951, NACA.

[2] Stein, G. D. and Wegener, P. P., "Experiments on the Number of Particles Formed by Homogeneous Nucleation in the Vapor Phase," *Journal of Chemical Physics*, Vol. 46, 1967, pp. 3685–3686.

[3] Stever, H. G., "Condensation Phenomena in High Speed Flows," *Fundamentals of Gas Dynamics*, edited by H. W. Em-

mons, Princeton Univ. Press, Princeton, N.J., 1958, pp. 526–573.
[4] Harding, L. J., "A Digital Computer Program for Condensation in Expanding One-Component Flows," Rept. ARL 65-58, March 1965, Aerospace Research Lab.

Motion of a Rigid Cylinder within a Shell-Core Structure

D. B. LONGCOPE*
Sandia Laboratories, Albuquerque, N.Mex.

Introduction

THE response of impulsively loaded, circular, elastic shells has recently received the attention of several investigators. A wave-type solution for the membrane stress in a long, circular shell subjected to a distributed impulse over one-half the shell circumference was derived in Ref. 1. For the same loading and shell configuration, a modal solution which includes both membrane and bending effects was obtained in Ref. 2. In Ref. 3, a solution for the axisymmetric, transient response of a long, circular shell containing an annular elastic core was presented.

In many applications, the response of elements within the shell structure must also be determined. This analysis is concerned with estimating the acceleration of a rigid cylinder within a shell-core structure when the shell is loaded by a pressure pulse distributed over one-half the shell circumference (see Fig. 1). The analysis considers a model in which the shell and core are treated as elastic; however, inertial effects in the core are neglected. Elasticity theory is used to obtain the spring effect of the core. Although wave propagation effects in the core are neglected, this simplification is supported by the fact that many core materials of interest, such as polyurethane foam, have low densities compared to the densities of other system elements.

Formulation

For a state of plane strain and neglecting shear deformation and rotatory inertia, the equations of motion, from Ref. 4, for the circular shell shown in Fig. 1 are

$$\frac{Kh^2}{12b^2}\left(\frac{\partial^4 w}{\partial\theta^4} + 2\frac{\partial^2 w}{\partial\theta^2} + w\right) + K\left(\frac{\partial v}{\partial\theta} + w\right) = -b^2\left[\rho h\frac{\partial^2 w}{\partial t^2} + \sigma_r(b,\theta) + q\right] \quad (1a)$$

$$K[(\partial^2 v/\partial\theta^2) + (\partial w/\partial\theta)] = b^2[\rho h(\partial^2 v/\partial t^2) + \tau_{r\theta}(b,\theta)] \quad (1b)$$

where w and v are the radial and tangential shell displacements; t is time; $\sigma_r(b,\theta)$ and $\tau_{r\theta}(b,\theta)$ are the core radial and shear stresses at the shell-core interface; $K = E_s h/(1 - \nu_s^2)$; ρ, h, b, E_s, and ν_s are the shell density, thickness, radius, Young's modulus, and Poisson's ratio, respectively; and the surface pressure q is given by

$$q = \begin{cases} p(t)\cos\theta, & |\theta| < \pi/2 \\ 0, & \pi/2 < |\theta| < \pi \end{cases} \quad (2)$$

The equation of motion for the rigid cylinder with density γ and radius a is

$$\pi a^2\gamma\frac{d^2x}{dt^2} = \int_0^{2\pi}[\tau_{r\theta}(a,\theta)\sin\theta - \sigma_r(a,\theta)\cos\theta]a\,d\theta \quad (3)$$

Received December 18, 1969. This work was supported by the U.S. Atomic Energy Commission. The author wishes to acknowledge the helpful suggestions of M. J. Forrestal and M. J. Sagartz.

* Staff Member.

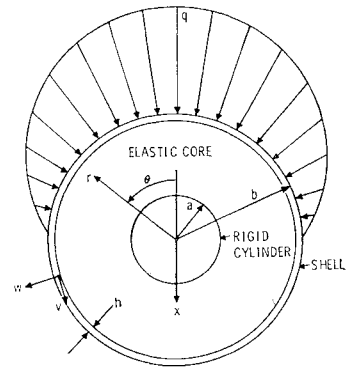

Fig. 1 Geometry of the problem.

where x is the displacement of the center of the rigid cylinder.

Solution

The applied pressure q, shell radial and tangential displacements w and v, and core stress components σ_r and $\tau_{r\theta}$ are expressed in series form as

$$q = p(t)\sum_{n=0}^{\infty} q_n\cos n\theta \quad (4a)$$

$$w = \sum_{n=0}^{\infty} w_n(t)\cos n\theta,\ v = \sum_{n=1}^{\infty} v_n(t)\sin n\theta \quad (4b)$$

$$\sigma_r = \sum_{n=0}^{\infty} S_n(r)\cos n\theta,\ \tau_{r\theta} = \sum_{n=1}^{\infty} T_n(r)\sin n\theta \quad (4c)$$

where r is the radial coordinate. The substitution of Eqs. (4) into Eqs. (1) and (3) results in a system of equations for each value of n. However, because of the orthogonality properties of the sine and cosine functions, only the system corresponding to $n = 1$ enters into the solution for the rigid cylinder displacement x. The equations for $n = 1$ are

$$K[v_1 + w_1] = -b^2[\rho h(d^2w_1/dt^2) + S_1(b) + q_1 p(t)] \quad (5a)$$

$$K[v_1 + w_1] = -b^2[\rho h(d^2v_1/dt^2) + T_1(b)] \quad (5b)$$

$$a\gamma(d^2x/dt^2) = T_1(a) - S_1(a) \quad (5c)$$

It should be noted that Eqs. (5) are identical to those that are obtained if the membrane theory of Ref. 1 is used to describe the shell response instead of Eqs. (1). In Eqs. (5), the coefficient q_1 is $\frac{1}{2}$. $S_1(r)$ and $T_1(r)$ are obtained by solving the $n = 1$ mode of the plane strain elasticity equations for the massless core, with continuity of displacements maintained at the shell-core ($r = b$) and core-rigid cylinder ($r = a$) interfaces. Then, in Eqs. (5),

$$S_1(b) = (G/b)(\sigma_1 w_1 + \sigma_2 v_1 + \sigma_3 x) \quad (6a)$$

$$T_1(b) = (G/b)(\tau_1 w_1 + \tau_2 v_1 + \tau_3 x) \quad (6b)$$

$$T_1(a) - S_1(a) = (G/a)(\delta_1 w_1 + \delta_2 v_1 + \delta_3 x) \quad (6c)$$

where

$$\sigma_1 = \frac{2}{\Gamma}\left[\frac{-2(3-2\nu)}{(3-4\nu)} + \frac{(4\nu^2 - 11\nu + 8)}{(3-4\nu)}k^{-2} - \frac{(4\nu^2 - 7\nu + 2)}{(3-4\nu)}k^2 - k^{-2}\ln k - (3-4\nu)k^2\ln k\right] \quad (6d)$$

$$\sigma_2 = \tau_1 = \frac{2}{\Gamma}\left[\frac{-2}{(3-4\nu)} - \frac{(4\nu^2 - 7\nu + 2)}{(3-4\nu)}k^{-2} + \frac{(4\nu^2 - 7\nu + 4)}{(3-4\nu)}k^2 - k^{-2}\ln k - (3-4\nu)k^2\ln k\right] \quad (6e)$$

$$\tau_2 = \frac{2}{\Gamma}\left[\frac{2(1-2\nu)}{(3-4\nu)} - \nu k^{-2} - \frac{(4\nu^2 - 7\nu + 2)}{(3-4\nu)}k^2 - k^{-2}\ln k - (3-4\nu)k^2\ln k\right] \quad (6f)$$